RESEARCH ARTICLE | JUNE 10 2025

Enhanced electrocaloric effect in lead-free relaxor ferroelectrics via point defect engineering

Zixuan Wu ; Wanting Hu ; Krishnarjun Banerjee ; Haixue Yan ; Man Zhang

Appl. Phys. Lett. 126, 232903 (2025)
https://doi.org/10.1063/5.0250512

Applied Physics Letters ARTICLE pubs.aip.org/aip/apl

Enhanced electrocaloric effect in lead-free relaxor ferroelectrics via point defect engineering

Cite as: Appl. Phys. Lett. **126**, 232903 (2025); doi: 10.1063/5.0250512
Submitted: 25 November 2024 · Accepted: 28 May 2025 ·
Published Online: 10 June 2025

Zixuan Wu,[1] Wanting Hu,[1] Krishnarjun Banerjee,[1] Haixue Yan,[1] and Man Zhang[2,a)]

AFFILIATIONS

[1]School of Engineering and Materials Science, Queen Mary University of London, Mile End Road, London E1 4NS, United Kingdom
[2]School of Mechanical Engineering, University of Leeds, Woodhouse, Leeds LS2 9JT, United Kingdom

[a)]Author to whom correspondence should be addressed: M.Zhang7@leeds.ac.uk

ABSTRACT

The electrocaloric effect enables solid-state refrigeration technology with high energy efficiency and zero global warming potential. Normal displacive ferroelectric materials exhibit the highest electrocaloric effect just above their Curie point. The freezing temperature (T_f) of a relaxor ferroelectric material functions as a Curie point in displacive ferroelectrics, suggesting that the highest electrocaloric effect for a relaxor ferroelectric material is near its T_f. However, relaxor ferroelectrics often exhibit significant hysteresis around T_f, making them unsuitable for electrocaloric applications. In this work, we show that the highest electrocaloric effect in lead-free $Bi_{0.5}Na_{0.5}TiO_3$-$SrTiO_3$-based relaxor ferroelectric ceramics occurs at temperatures a few degrees above the temperature with their maximum permittivity (T_m) and is far above their T_f. Moreover, the A-site vacancy design can be used to effectively increase the electrocaloric effect and broaden the working temperature range, which is due to the increase in field-induced polarization and strong relaxation achieved via point defect engineering. This Letter reveals the appropriate temperature window for the high electrocaloric effect in relaxor ferroelectrics and shows that the A-site vacancy design can further enhance electrocaloric properties and extend the working temperature range for electrocaloric applications.

Electrocaloric materials hold significant promise as core components in solid-state refrigeration technologies. Compared to traditional vapor-compression refrigeration, which has long been criticized due to greenhouse gas emissions,[1,2] electrocaloric refrigeration is more energy-efficient and has zero global warming potential. Electrocaloric refrigeration describes the reversible adiabatic temperature change (ΔT) occurring in dielectric materials during the application or removal of electric fields.[3–5] Among various dielectric materials, ferroelectrics exhibit the largest ΔT due their large electric field-induced polarization change. However, ferroelectrics are not readily used in electrocaloric devices due to the following factors: (1) narrow working temperature window: Conventional displacive ferroelectrics show the largest ΔT just above their Curie point (T_C), with ΔT decreasing sharply as temperatures depart from T_C,[1,2] leading to a narrow working temperature window; (2) the absence of lead-free materials with high performance: Currently, the ferroelectric system $Pb(Sc_{1/2}Ta_{1/2})O_3$ has exhibited the highest ΔT (3.7 K at 40 kV cm^{-1}) at room temperature[6,7] among all ferroelectrics studied so far. However, this material contains lead, which is toxic, and scandium, which is expensive. Thus, it is urgent to develop lead-free ferroelectrics with high ΔT and wide working temperature range near room temperature.

Relaxor ferroelectrics, which contain polar nano-regions (PNRs) and exhibit broad and temperature-dependent dielectric permittivity peaks, have the potential to provide a wide working temperature range.[2,8–10] The PNRs, which are randomly oriented, exist over a wide temperature range between the freezing temperature (T_f) and Burns temperature (T_B). The T_f describes the temperature where short-range ordered PNRs transform into long-range ordered domains under applied DC fields. The T_B describes the temperature where PNRs begin to form during cooling. Upon the application of an electric field, randomly oriented PNRs align along the electric field direction and cause large polarization change, enabling high electrocaloric effect across a wide working temperature range. Currently, most research on relaxor ferroelectrics for electrocaloric applications is centered on compositions with a T_f near room temperature, where T_f here is comparable to T_C in normal ferroelectrics. However, relaxor ferroelectrics often exhibit significant hysteresis around their T_f due to field-induced transitions from relaxor ferroelectrics to displacive ferroelectrics, leading to

reduced efficiency and shorter lifetime for electrocaloric devices.[11,12] Thus, it is crucial to clarify the optimal working temperature range for lead-free relaxor ferroelectrics.

$Bi_{0.5}Na_{0.5}TiO_3$ (BNT) is the most widely studied lead-free relaxor ferroelectric, characterized by a large spontaneous polarization. However, its T_f is far above room temperature (near 190 °C).[13] $SrTiO_3$ (ST) is a quantum paraelectric that shows Curie point near 0 K.[14] By introducing ST into BNT, the T_f values of BNT-ST solid solutions could be effectively reduced to near or below room temperature, allowing the investigation of the electrocaloric effect above T_f. Specifically, the temperature change in electrocaloric effect is proportional to the change of polarization with temperatures under an applied electric field,[15,16] indicating that the electrocaloric effect is related to polarization instabilities. It has been proven that Schottky defects in ferroelectrics can effectively influence the stability of polarization and increase dielectric tunability.[17] It is possible to use the defect engineering design to enhance the electrocaloric performance of ferroelectric materials. In this work, A-site vacancies were introduced in BNT-ST solid solutions via point defect engineering to enhance the electrocaloric effect.

The ceramic samples in this work have chemical formula of $Sr_x(Bi_{1-x}Na_{0.97-x}Li_{0.03})_{0.5}TiO_3$ (x = 0.42, 0.48, and 0.52, named as BNT-100xST), where Sr, Bi, Na, and Li are on the A site and Ti is on the B site of the ABO_3 perovskite structure. Another composition with chemical formula of $[Sr_x(Bi_{1-x}Na_{0.97-x}Li_{0.03})_{0.5}]_{0.99}TiO_{3-\delta}$ is prepared, where x = 0.48 and the atom ratio of A- to B-site is 0.99, named as BNT-48ST-0.99. All the ceramics were prepared by the solid-state reaction method. In BNT-48ST-0.99 ceramics, the A/B ratio of 0.99 was chosen according to Ref. 17, where the highest figure of merit calculated from tunability and loss is achieved when the (Ba + Sr)/Ti ratio equals to 0.99 in the $BaTiO_3$–$SrTiO_3$ system. The raw materials, including $SrCO_3$ (Sigma-Aldrich, ≥99.9%), Bi_2O_3 (Sigma-Aldrich, ≥99.9%), Na_2CO_3 (Sigma-Aldrich, ≥99.5%), Li_2CO_3 (Sigma-Aldrich, ≥99.0%), and TiO_2 (Sigma-Aldrich, ≥99.8%), were dried at 200 °C overnight, followed by weighing according to stoichiometric ratios and mixing by ball milling. The ball-milled slurries were dried and subsequently calcined at 800 °C for 2 h and then 900 °C for 2 h to drive the chemical reactions needed to obtain the designed compositions. After that, ball-milling was repeated to obtain fine and uniform particles. After the addition of 5 wt. % polyvinyl alcohol, the powder was pressed into pallets and heated at 650 °C for 2 h to remove the binder. The green compacts were sintered at 1150 °C for 4 h.

The crystal structure of the samples at room temperature was investigated by x-ray diffraction (XRD, Xpert-Pro). XRD data were fitted using GSAS-II software.[18] The microstructure and composition homogeneity of the samples were characterized by scanning electron microscopy (SEM, FEI Inspect F) and energy dispersive x-ray spectroscopy (EDS). Surface chemical analysis was conducted by x-ray photoelectron spectroscopy (XPS, ThermoFisher Nexsa). All the spectra were calibrated using C 1s peak and fitted using the Gaussian–Lorentzian function. The temperature dependence of heat capacity was acquired by differential scanning calorimetry (DSC, DSC 25) with the controlled heating rate (2 °C/min) in the temperature range from 0 to 100 °C. The density of all ceramic samples was obtained using the Archimedes' principle in water. The relative density of all ceramics was obtained through the ratio of measured density to theoretical density, which was determined using the molar mass of the developed compositions and unit cell volume from XRD refinement. Prior to electrical tests, Ag electrodes (SunChemical Ltd.) were fired on both sides of the samples. The temperature dependence of dielectric permittivity and loss was measured by an LCR meter (Agilent, 4284A) connected to a furnace. The hysteresis loops were measured at 10 Hz and different temperatures in silicone oil by using a ferroelectric hysteresis measurement tester (NPL, UK).

The relative density of all sintered ceramics was higher than 95%. Figures S1–S4 show SEM and EDS results of BNT-ST ceramics. All the ceramics show good crystallinity and low porosity, confirming good sintering quality. The EDS results reveal a homogeneous elemental distribution within all samples.

Figures 1(a)–1(d) show the XRD patterns of BNT-ST crushed powder from the sintered ceramics, with enlarged peaks from (110), (200), and (211) planes. The XRD patterns and fitted profiles through Rietveld refinement are shown in Fig. S5. All the ceramics were determined to possess a perovskite structure without impurities, while exhibiting tetragonal (space group: *P4bm*) and cubic (space group: *Pm-3m*) symmetries according to the Rietveld refinement. The goodness of fit (GOF χ^2) values indicate that the Rietveld refinements of BNT-ST ceramics are reliable. The phase compositions and refined lattice parameters are listed in Table SI. As indicated in the figures, higher ST content leads to lower percentage of polar tetragonal phase in the samples, which can be attributed to the cubic structure of ST.[19,20] Moreover, comparing BNT-48ST and BNT-48ST-0.99 samples, the introduction of A-site vacancy causes an increase in the percentage of the polar phase (64.2%). This is also supported by Figs. 1(e)–1(j), where the peak intensity of the polar tetragonal phase (cyan bar) increases relative to the cubic phase (magenta bar) in the BNT-48ST-0.99 sample. However, the lattice distortion of all ceramics remains consistent, close to 1.414. This is obtained by the a/c ratio for the

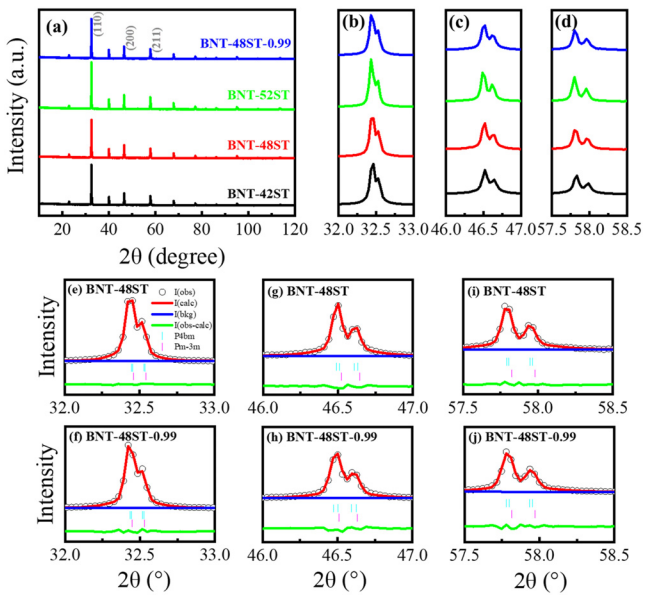

FIG. 1. (a) XRD patterns of BNT-ST ceramics at room temperature. (b)–(d) Enlarged views of three strong peaks in the local regions around 2θ = (b) 32.3°, (c) 46.4°, and (d) 57.7°. (e)–(j) Enlarged views of the same peak regions in the diffractograms of BNT-48ST and BNT-48ST-0.99 ceramics.

tetragonal phase *P4bm* with lattice parameters of $a_T \sim \sqrt{2}c_c$ and $c_T \sim c_c$, where a_T, c_T, and c_c are the lattice parameters of tetragonal and cubic structures, respectively.[18] However, XRD data alone are not enough to confirm structural changes in the BNT-based system. In this work, dielectric and ferroelectric methods were used to support the discussions on phase transitions.[13,21,22]

Figure 2 shows the temperature dependence of dielectric permittivity and loss for BNT-ST ceramics. Frequency-dependent broad peaks for both dielectric permittivity and loss were observed for all samples, which are typical characteristics of relaxor ferroelectrics. As the ST content increases, the permittivity peaks become broader, indicating that ST can effectively disrupt the long-range ferroelectric order, as also supported by decreased temperature values with the maximum permittivity (T_m). Meanwhile, the dielectric permittivity decreases by increasing the ST content, in good agreement with XRD results that showing a reduced percentage of the tetragonal phase.[23] All three compositions with an atomic ratio A/B = 1 share similar dielectric loss behavior.

As shown in Fig. S6, the introduction of A-site vacancy causes a decrease in both permittivity and loss near room temperature, even though XRD results show a higher proportion of the tetragonal phase in BNT-48ST-0.99 ceramics. This is possibly related to the fact that the A-site vacancies are charge-balanced by oxygen vacancies, which exert a pinning effect on PNRs, thereby reducing their dielectric activity.[17] However, it is worth noting that the BNT-48ST-0.99 sample exhibits a broader temperature-dependent permittivity peak, indicating that the introduction of A-site vacancy increases the material's relaxation by increasing structural disorder.[3]

TABLE I. The characterized temperatures and γ value of BNT-ST ceramics.

Composition	T_f (°C)	T_m (°C) (100 Hz)	ΔT_m (°C) (100 Hz–100 kHz)	γ
BNT-42ST	−13.26	56.67	32.80	1.54
BNT-48ST	−41.40	34.02	33.91	1.63
BNT-52ST	−51.73	25.91	35.21	1.68
BNT-48ST-0.99	−25.07	45.71	35.18	1.79

To better examine the relaxation behavior, Vogel–Fulcher (V–F) and modified Curie–Weiss (C–W) fittings were performed, using the dielectric permittivity data at different frequencies. The fitted plots are shown in Fig. S7, and the key parameters are summarized in Table I. Since the transition between different dipole orientations is a thermally activated process, the frequency (f) will partially satisfy the V–F law,

$$f = f_0 e^{-\frac{E_a}{k(T_m - T_f)}} \quad (1)$$

where f represents the frequencies where relaxation occurs, f_0 is the attempt frequency, E_a is the activation energy required for dipole reorientation, and k is the Boltzmann constant. The fitted T_f indicates the temperature of dipole freezing.[24,25] The dielectric permittivity measured at 100 kHz was selected for the modified C–W law fitting,

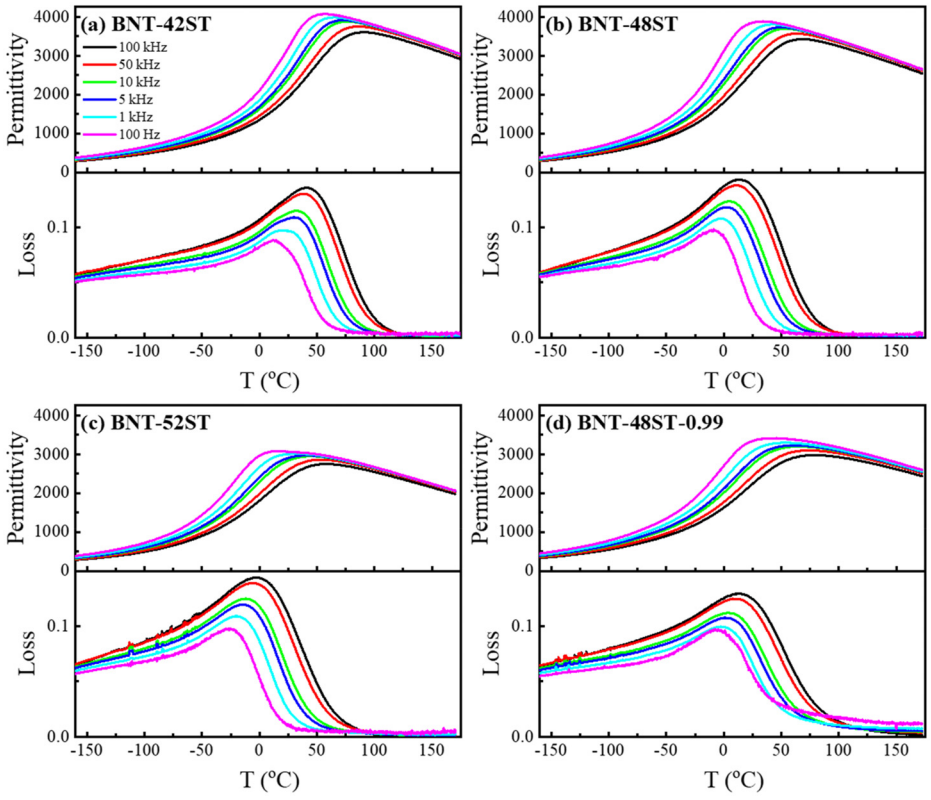

FIG. 2. Temperature dependence of dielectric permittivity and loss of (a) BNT-42ST, (b) BNT-48ST, (c) BNT-52ST, and (d) BNT-48ST-0.99 ceramics.

$$\frac{1}{\varepsilon}-\frac{1}{\varepsilon_m}=\frac{(T-T_m)^{\gamma}}{C}, \tag{2}$$

where C is the Curie–Weiss constant, which is within the same order of 10^5 K for relaxor ferroelectrics; γ is a parameter that is used to describe the diffuseness of a transition, where $\gamma = 2$ for ideal diffuse-type phase transitions.[24,26]

As shown in Fig. S7 and Table I, by increasing the ST content, the transition temperatures T_f and T_m of BNT-ST ceramics decrease, while the relaxation behavior increases, consistently with the increment of ΔT_m (difference in T_m between 100 Hz and 100 kHz) and γ values. Additionally, the introduction of A-site vacancy and defect dipoles led to an increase in T_f and T_m, as well as relaxation strength ΔT_m and the γ value. The increase in ΔT_m and γ values further suggest that the introduction of A-site vacancy enhances the relaxation behavior of the sample, which may enable to increase the working temperature range for electrocaloric applications.

Figure 3 shows the XPS O1s spectra of BNT-ST ceramics. The three peaks from low to high energy in O element mapping correspond sequentially to lattice oxygen, oxygen associated with nearby vacancies, and surface adsorbed oxygen.[27] As the ST content increases, oxygen vacancy is always present in the samples at almost consistent level. However, by comparing Figs. 3(b) and 3(d), it results evident that the introduction of A-site vacancies causes a significant increase in the content of oxygen vacancies, compared to the sample without intentionally introduced defects. According to the following point defect reaction equation:[17]

$$TiO_2 \xrightarrow{(Bi,Na,Sr)TiO_3} Ti_{Ti}^{X} + 2O_O^X + V''_{Bi,Na,Sr} + V_O^{\cdot\cdot}. \tag{3}$$

A-site vacancies are mainly balanced through ionic charge compensation by oxygen vacancies, which greatly influence the dielectric and ferroelectric properties of the samples.

The electrocaloric effect can be obtained either by an indirect method based on the Maxwell's relations in adiabatic reversible systems that can be transformed as a function of the electric field or by the direct method, which involves thermal measurements. The indirect method is employed much more frequently than the direct method.[28] The applicability and accuracy of the indirect method in relaxor ferroelectrics have been often questioned due to the so-called memory effect.[1,15] In the ergodic state (at temperatures above T_f), the indirect method remains valid due to the absence of latent heat during the phase transition.[1] Indeed, studies on relaxor ferroelectric systems, including in BNT-based materials, show that the electrocaloric effect measured by the indirect and direct methods is almost the same in the ergodic state.[11,29]

Figure S8 shows the polarization–electric field (P–E) loops of BNT-ST ceramics at different temperatures. All the ceramics exhibit slim P–E loops, which is a typical feature of relaxor ferroelectrics in the ergodic state. At the same temperature, the maximum polarization in the samples gradually decreases as the ST content increases, due to the decreased percentage of the tetragonal phase.[23] In contrast, the BNT-48ST-0.99 sample exhibits a higher maximum polarization under the same conditions, which can be attributed to its relatively higher

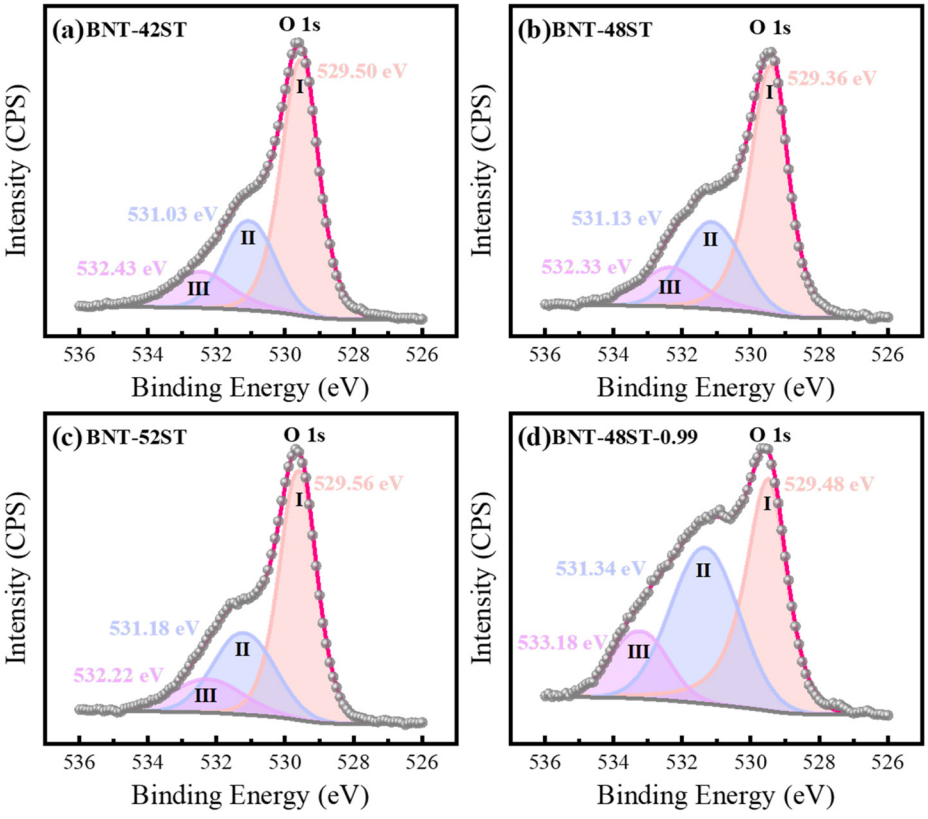

FIG. 3. XPS O1s spectra of (a) BNT-42ST, (b) BNT-48ST, (c) BNT-52ST, and (d) BNT-48ST-0.99 ceramics.

concentration of the polar phase. Figure 4(a) shows the temperature dependence of the polarization under an electric field of 5 kV/mm, which was calculated from the data in Fig. S8. The polarization decreases with increasing ST concentration, consistent with the XRD results shown in Table SI. However, the composition modified by point defect engineering shows the highest maximum polarization.

Figure 4(b) shows the variation of ΔT in all compositions as a function of temperature. The ΔT is estimated using the Maxwell's relations as follows:

$$\Delta T = \int_{E_1}^{E_2} -\frac{T}{\rho C}\left(\frac{\partial P}{\partial T}\right)_E dE, \tag{4}$$

where E is the electric field, E_1 and E_2 are 0 and 5 kV/mm, respectively, T is the temperature, ρ is the density, and C is the heat capacity. ρ and C were obtained by the Archimedes' principle and DSC in Fig. S9, respectively. In particular, C values being used for calculation are temperature-dependent values across the temperature range between 20 and 80 °C.[16] Figures 4(c) and S10 show the temperature and electric field dependence of the pyroelectric coefficient of BNT-ST ceramics. All BNT-ST solid solutions show a broad temperature for the electrocaloric effect. By increasing the ST content, the temperatures corresponding to the largest electrocaloric effect (the highest ΔT) shift to lower values, consistently with the decrease in T_f and T_m. It is worth highlighting that the temperature corresponding to the highest electrocaloric effect in each relaxor ferroelectric is just above their T_m (measured at 100 Hz) rather than T_f, even though T_f for relaxor ferroelectrics functions as T_C for normal ferroelectrics. This is attributed to the low stability of the polar structure above T_f. Moreover, BNT-48ST-0.99 ceramics show not only a wider working temperature range but also a higher electrocaloric effect. It is worth noting that introduced A-site vacancy led to an upward shift in the characterized temperatures (T_f and T_m), potentially suppressing the enhanced electrocaloric effect of BNT-48ST-0.99 sample within certain temperature ranges. Compared to the stoichiometric sample, the sample with A-site vacancy exhibits an increased working temperature range. In literature, the temperature span (T_{span}, $\Delta T \geq 0.8\Delta T_{max}$) is used to evaluate the working temperature range of electrocaloric materials.[30,31] In this work, we also use the temperature span (T_{span}) to describe working temperature range of our developed materials. Compared to the BNT-48ST sample, the BNT-48ST-0.99 sample shows an increase in T_{span} from 19.28 to 21.38 K and an enhancement in the electrocaloric effect from 0.37 to 0.46 K. The wide working temperature range is related to its high relaxation strength ΔT_m and the γ value. The highest peak of the electrocaloric effect can be attributed to its high field-induced polarization associated with the instability of its polar structures under a high applied field, which can generate larger temperature change.

Figure 4(d) illustrates the differences in the electrocaloric effect near T_f and T_m of a relaxor ferroelectric, using polarization and microstructural changes under a high electric field. At temperatures just above T_f, the applied electric field can induce a phase transition, during which PNRs grow into large-sized polar structures. This process is accompanied by high loss, as visible in the P–E loop, making the material unsuitable for electrocaloric applications near T_f. With increasing temperature, the polarization and stability of PNRs decrease. While a decrease in polarization is unfavorable for achieving a high ΔT, a decrease in the stability in PNRs contributes to high ΔT. At temperatures between T_f and just above T_m, the contribution from the instability of PNRs overcomes that from decreased polarization, leading to the maximum ΔT at temperatures just above T_m. Moreover, the slim P–E loops in this temperature range indicate low loss, high efficiency, and longer life cycles for electrocaloric devices. When the temperature is much higher than T_m, the contribution from decreased polarization takes over, and the ΔT decreases with a further temperature increase. By introducing A-site vacancy into a relaxor ferroelectric, the relaxation behavior of the material is further enhanced, which is beneficial

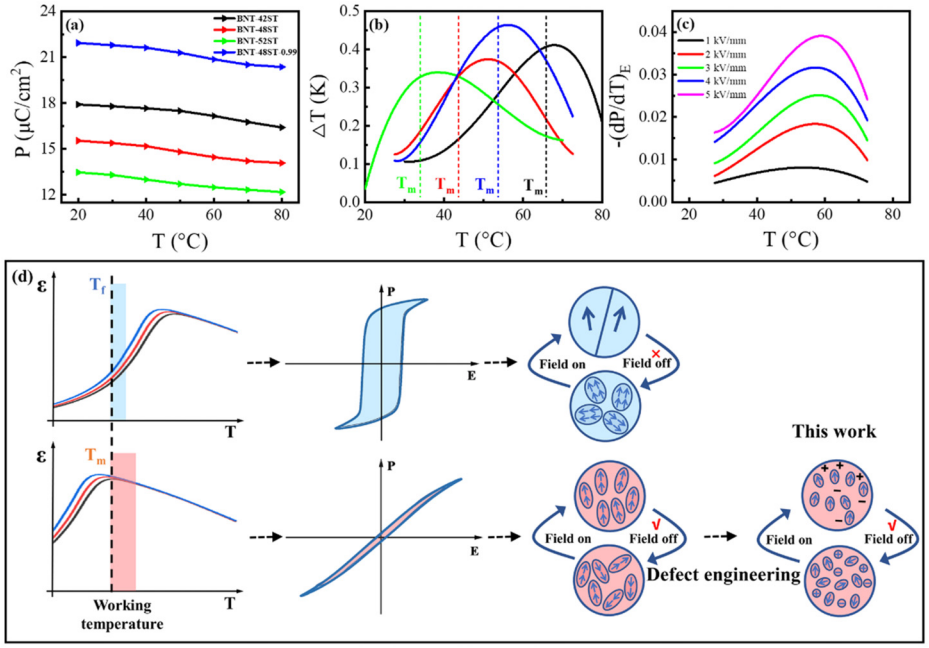

FIG. 4. Temperature dependence of (a) polarization and (b) ΔT of BNT-ST ceramics under an electric field of 5 kV/mm; (c) temperature and electric field dependence of the pyroelectric coefficient of BNT-48ST-0.99 ceramics; and (d) schematic representation of permittivity and polarization mechanisms to achieve high electrocaloric effect in relaxor ferroelectrics through point defect engineering.

for improving the electrocaloric effect and broadening the working temperature range.

In conclusion, BNT-ST ceramics were prepared by the solid-state reaction method and provided a wide working temperature range near room temperature for electrocaloric applications. All ceramics exhibited relaxor behavior with the peak temperature for the electrocaloric effect occurring just above T_m and well above T_f. Moreover, the modulation of A/B site atomic ratio through the introduction of A-site vacancies can significantly extend the working temperature range for electrocaloric applications and increase the peak intensity of electrocaloric effect, due to high relaxation strength and increased field-induced polarization. This study highlights the potential of defect engineering in relaxor ferroelectrics to improve electrocaloric properties.

See the supplementary material for the SEM images, EDS maps, XRD refined data and parameters, selected and fitted dielectric data, P–E loops, and temperature dependent heat capacity of BNT-ST ceramics.

Z.W. and W.H. acknowledge the financial support from China Scholarship Council scholarship (CSC, Nos. 202207000015 and 202106370015). K.B. acknowledges the financial support from the Engineering and Physical Sciences Research Council (RC Grant reference: EP/Y027752/1), and M.Z. acknowledges the finical support from the Royal Society of Chemistry (RG. MECH.133627).

AUTHOR DECLARATIONS

Conflict of Interest

The authors have no conflicts to disclose.

Author Contributions

Zixuan Wu: Conceptualization (equal); Data curation (lead); Formal analysis (equal); Investigation (lead); Validation (lead); Visualization (lead); Writing – original draft (lead); Writing – review & editing (equal). **Wanting Hu:** Formal analysis (equal); Methodology (lead); Writing – review & editing (equal). **Krishnarjun Banerjee:** Formal analysis (equal); Methodology (equal); Writing – review & editing (equal). **Haixue Yan:** Conceptualization (equal); Funding acquisition (equal); Supervision (equal); Writing – review & editing (equal). **Man Zhang:** Conceptualization (equal); Funding acquisition (equal); Supervision (equal); Writing – review & editing (equal).

DATA AVAILABILITY

The data that support the findings of this study are available from the corresponding author upon reasonable request.

REFERENCES

[1]M. Valant, Prog. Mater. Sci. **57**(6), 980 (2012).
[2]J. Shi, D. Han, Z. Li, L. Yang, S.-G. Lu, Z. Zhong, J. Chen, Q. M. Zhang, and X. Qian, Joule **3**(5), 1200 (2019).
[3]G. Li, F. Yan, K. Zhu, C. Shi, G. Ge, J. Lin, Y. Shi, B. Shen, and J. Zhai, Acta Mater. **227**, 117750 (2022).
[4]W. Lin, G. Li, J. Qian, G. Ge, S. Wang, J. Lin, J. Lin, B. Shen, and J. Zhai, ACS Nano **18**(20), 13322 (2024).
[5]C. H. Lei and Y. Liu, Appl. Phys. Lett. **121**(10), 102902 (2022).
[6]Y. Nouchokgwe, P. Lheritier, C. H. Hong, A. Torello, R. Faye, W. Jo, C. R. H. Bahl, and E. Defay, Nat. Commun. **12**(1), 3298 (2021).
[7]J. Li, A. Torelló, V. Kovacova, U. Prah, A. Aravindhan, T. Granzow, T. Usui, S. Hirose, and E. Defay, Science **382**(6672), 801 (2023).
[8]J. Li, R. Yin, Y. Hou, Z. Xiong, Y. Wang, H. Cheng, X. Su, X. Zhang, W. Wu, L. Li, and Y. Bai, Appl. Phys. Lett. **125**(15), 152904 (2024).
[9]M. Otoničar, A. Bradeško, L. Fulanović, T. Kos, H. Uršič, A. Benčan, M. J. Cabral, A. Henriques, J. L. Jones, L. Riemer, D. Damjanovic, G. Dražić, B. Malič, and T. Rojac, Adv. Funct. Mater. **30**(52), 2006823 (2020).
[10]A. Kumar, J. N. Baker, P. C. Bowes, M. J. Cabral, S. Zhang, E. C. Dickey, D. L. Irving, and J. M. LeBeau, Nat. Mater. **20**(1), 62 (2021).
[11]L. Wen, J. Yin, X. Wu, X. Wei, W. Liu, D. Yang, and J. Wu, Acta Mater. **255**, 119090 (2023).
[12]N. Zeggai, B. Dkhil, M. LoBue, and M. Almanza, Appl. Phys. Lett. **122**(8), 081903 (2023).
[13]B. N. Rao, R. Datta, S. S. Chandrashekaran, D. K. Mishra, V. Sathe, A. Senyshyn, and R. Ranjan, Phys. Rev. B **88**(22), 224103 (2013).
[14]T. Sakudo and U. H, Phys. Rev. Lett. **26**(14), 851 (1971).
[15]Y. Liu, J. F. Scott, and B. Dkhil, Appl. Phys. Rev. **3**(3), 031102 (2016).
[16]D. Gracia, S. Lafuerza, J. Blasco, and M. Evangelisti, APL Mater. **11**(12), 121101 (2023).
[17]T. Teranishi, R. Kanemoto, H. Hayashi, and A. Kishimoto, J. Am. Ceram. Soc. **100**(3), 1037 (2017).
[18]G. O. Jones and P. A. Thomas, Acta Crystallogr., B **B58**, 168 (2002).
[19]X. Zhou, G. Xue, H. Luo, C. R. Bowen, and D. Zhang, Prog. Mater. Sci. **122**, 100836 (2021).
[20]G. Viola, Y. Tian, C. Yu, Y. Tan, V. Koval, X. Wei, K.-L. Choy, and H. Yan, Prog. Mater. Sci. **122**, 100837 (2021).
[21]C. Ma and X. Tan, Solid State Commun. **150**(33–34), 1497 (2010).
[22]C. Ma, H. Guo, S. P. Beckman, and X. Tan, Phys. Rev. Lett. **109**(10), 107602 (2012).
[23]S. C. Abrahams, S. K. Kurtz, and P. B. Jamieson, Phys. Rev. **172**(2), 551 (1968).
[24]H. Zhang, B. Yang, A. D. Fortes, H. Yan, and I. Abrahams, J. Mater. Chem. A **8**(45), 23965 (2020).
[25]K. B. Lyons, P. A. Fleury, and D. Rytz, Phys. Rev. Lett. **57**(17), 2207 (1986).
[26]K. Uchino and S. Nomura, Ferroelectrics **44**(1), 55 (1982).
[27]B. Wang, R. S. Alazwari, S. Ahmed, Z. Hu, M. J. Cattell, and H. Yan, Dent. Mater. **40**(6), 921 (2024).
[28]X. Chen, S. Li, X. Jian, Y. Hambal, S.-G. Lu, V. V. Shvartsman, D. C. Lupascu, and Q. M. Zhang, Appl. Phys. Lett. **118**(12), 122904 (2021).
[29]F. L. Goupil, A. Berenov, A.-K. Axelsson, M. Valant, and N. M. Alford, J. Appl. Phys. **111**(12), 124109 (2012).
[30]R. Yin, J. Li, X. Su, S. Qin, C. Yu, Y. Hou, C. Liu, Y. Su, L. Qiao, T. Lookman, and Y. Bai, Adv. Funct. Mater. **32**(5), 2108182 (2021).
[31]F. Li, X. Ji, X. Wang, C. Dai, X. Wang, S. Chen, W. Liu, M. Long, L. Shan, H. Qi, J. Wang, C. Wang, and Z. Cheng, Adv. Funct. Mater. **35**(16), 2418534 (2024).